Showcasing work by Prof. Chung-Yuan Mou's group and Prof. Heng-Liang Wu's group from the Center for Condensed Matter Sciences (CCMS) in National Taiwan University, Taiwan.

Advanced nanoporous separators for stable lithium metal electrodeposition at ultra-high current densities in liquid electrolytes

Inorganic mesoporous MSTF/AAO separator with straight nanopores regulates lithium ion flux and exhibits stable lithium plating and stripping processes in Li metal batteries.

As featured in:

See Chung-Yuan Mou, Heng-Liang Wu *et al.*, *J. Mater. Chem. A*, 2020, **8**, 5095.

ROYAL SOCIETY
OF **CHEMISTRY**

rsc.li/materials-a

ROYAL SOCIETY
OF CHEMISTRY

PAPER

Check for updates

Advanced nanoporous separators for stable lithium metal electrodeposition at ultra-high current densities in liquid electrolytes†

Jingling Yang,[ab] Chun-Yao Wang,[ac] Chun-Chieh Wang,[d] Kuei-Hsien Chen,[ace] Chung-Yuan Mou (ID) *[af] and Heng-Liang Wu (ID) *[ag]

Lithium metal anodes form a dendritic structure after cycling which causes an internal short circuit in flammable electrolytes and results in battery fires. Today's separators are insufficient for suppressing the formation of lithium dendrites. Herein, we report on the use of mesoporous silica thin films (MSTFs) with perpendicular nanochannels (pore size ∼5 nm) stacking on an anodic aluminum oxide (AAO) membrane as the MSTF⊥AAO separator for advancing Li metal batteries. The nanoporous MSTF⊥AAO separator with novel inorganic structures shows ultra-long term stability of Li plating/stripping in Li–Li cells at an ultra-high current density and capacity (10 mA cm^{-2} and 5 mA h cm^{-2}). A significant improvement over the state-of-the-art separator is evaluated based on three performance indicators, *e.g.* cycle life, current density and capacity. In Li–Cu cells, the MSTF⊥AAO separator shows a coulombic efficiency of >99.9% at a current density of 10 mA cm^{-2} for more than 250 h of cycling. The separator gives improved rate capability in Li–LiFePO$_4$ (LFP) batteries. The excellent performance of the MSTF⊥AAO separator is due to good wetting of electrolytes, straight nanopores with negative charges, uniform Li deposition and blocking the finest dendrite.

Introduction

Lithium (Li) metal is considered as the ultimate anode material for the development of next-generation batteries, mainly due to its extremely high theoretical specific capacity (3860 mA h g^{-1} *vs.* 372 mA h g^{-1} for graphite), the most electronegative potential and the lightest weight, compared to other alkali metals.[1] However, Li metal as an anode material for Li metal batteries still suffers from some serious drawbacks. First, active Li metal reacts with aprotic liquid electrolytes easily and forms a porous and inhomogeneous solid electrolyte interphase (SEI) layer on the Li metal surface.[1,2] The highly resistive SEI layer is associated with performance degradation and the dendrite

formation.[3] Second, Li electrodes form dendritic structures and isolated Li particles (dead Li) after electroplating and stripping processes which causes an internal short circuit and rapid heating of the cell.[1,2,4] Li dendrite growth could result from the inhomogeneous ion transport to the Li metal surface.

To achieve practical Li metal battery applications, various strategies based on modification of electrolytes, electrodes, and separators have been explored.[5,6] Different liquid electrolytes and additives have been used to suppress the growth of Li dendrites and improve the interfacial stability of the SEI layer on Li electrodes.[7,8] However, most electrolyte additives would be continuously consumed during cycling so that the effect of electrolyte additives on Li metal is not fully sustainable. In most cases, the stability of Li can be improved at small current densities and low capacities. The formation of Li dendrites would still exist in cells operating at high current densities. For the development of rechargeable Li metal batteries, eliminating the formation of Li dendrites and the risk of internal shorts at practical currents and areal capacities are still challenging. The relevant material designs such as polymers, solid-state electrolytes or solid-state blocking layers pre-coated on the Li surface have been proposed to block Li dendrites.[2,9]

Separators serve the function of separating the anode and the cathode to prevent Li dendrite penetration while ensuring sufficient passage of the Li ion and electrolyte.[5] An ideal separator would be thermally stable, highly ionic conducting, and impenetrable to dendrite growth. Traditional polyolefin

[a]*Center for Condensed Matter Sciences, National Taiwan University, Taipei 10617, Taiwan. E-mail: cymou@ntu.edu.tw; hengliangwu@ntu.edu.tw*

[b]*School of Environment, Jinan University, Guangzhou 510632, China*

[c]*Department of Chemistry, National Taiwan Normal University, Taipei 106, Taiwan*

[d]*National Synchrotron Radiation Research Center, Hsinchu, 30076, Taiwan*

[e]*Institute of Atomic and Molecular Sciences, Academia Sinica, Taipei 10617, Taiwan*

[f]*Department of Chemistry, National Taiwan University, Taipei 10617, Taiwan*

[g]*Center of Atomic Initiative for New Materials, National Taiwan University, Taipei 10617, Taiwan*

separators have many drawbacks such as non-wetting of electrolyte, large pore size and poor thermal stability, which are insufficient for practical Li metal battery applications.[5] The use of porous inorganic materials, such as glass fibers and porous Al_2O_3, with high hydrophilicity and high thermal stability at elevated temperature has been proposed to block Li dendrites and effectively improve safety of Li metal batteries.[9] However, their pore sizes are normally above the range of tens of nanometers which are insufficient for stopping dendrite penetration at high current density.

Our approach is to make a separator whose pore size is in the sub-10 nm range such that it is surely smaller than any conceivable Li dendrite diameter. At the same time, the thickness of this sub-10 nm pore film needs to be as small as possible, preferably in tens of nanometers, so as not to impede the ionic conductivity. We grew mesoporous silica thin films (MSTFs) with perpendicular nanochannels onto the 70 nm pore-size anodic aluminum oxide (AAO) membrane as the MSTF⊥AAO separator for Li metal batteries. AAO only serves as a support in this study. High quality continuous thin films of mesoporous silica with vertical pores are formed with a film thickness of *ca.* 30 nm and uniform pore diameters of 5.4 ± 0.4 nm. The ordered vertical nanochannels with charged walls are expected to block Li dendrites effectively. The designed porous MSTF⊥AAO separator has several nice features for a good separator, including good wetting of electrolytes (CA ≈ 0°), thermal stability, ultra-small pore size, high porosity with low tortuosity ($\tau \approx 1$), and charged pore channels. A separator is not just a passive blocking device in batteries, it can also be designed to control the ionic current for stable batteries.[10]

In our MSTF⊥AAO separator, the current/ion distribution would be very uniform both in the *z*-direction (perpendicular to anode) and *x*, *y* direction. As a result, we achieved ultra-long life performance in Li–Li symmetric cells at record high current densities (10–20 mA cm⁻²) and flat Li deposition at electrodes with the MSTF⊥AAO separator. The MSTF⊥AAO separator shows a significant improvement over the state-of-the-art separator and its performance is evaluated based on three performance indicators, *e.g.* cycle life, current density and capacity. We also studied the enhanced coulombic efficiency (CE) of Li–Cu cells so that future application of the separator in anode-free batteries could be evaluated. Finally, we demonstrate an enhanced full Li metal battery performance cycled at a high discharge–charge rate using the MSTF⊥AAO separator, Li metal anode and LiFePO₄ (LFP) cathode.

Results and discussion

A highly ordered mesoporous silica thin film (MSTF) of continuous macroscopic dimension was synthesized on top of anodic aluminum oxide (AAO) through a polymer transfer method. The perpendicular nanochannels with a pore size of ~5 nm regulate the Li plating/stripping behavior and improve the stability of Li metal batteries. Details of the preparation methods are provided in the Experimental section and ESI.† Fig. 1A shows a schematic diagram of the structure of the anodic aluminum oxide (AAO) substrate with periodic straight-through macropores. Fig. 1B shows a schematic diagram of the structure of the MSTF on the AAO membrane (MSTF⊥AAO). Scanning electron microscopy (SEM) images in Fig. 1C–E show the top view and cross sectional view of the bare AAO membrane, demonstrating periodic macropore channels of *ca.* 70 nm. The top-view SEM images of the MSTF⊥AAO membrane (Fig. 1F, G) show the continuous periodic nature of the mesoporous silica thin film (MSTF) with perpendicular pores on the AAO support and without apparent defects or breaks. Under SEM observation, the MSTF is a translucent single layer with extremely uniform pore size (5.4 ± 0.4 nm). One can clearly see the perpendicular pore structure of the MSTF covering the underlying AAO substrate (Fig. 1G). SEM images of the cross-sectional view of MSTF⊥AAO reveal the ultrathin smooth layer of the MSTF on top of the AAO surface (Fig. 1H). The MSTF has a uniform thickness of ~30 nm and the AAO support has the uniform perpendicular channels of length of ~56 μm (Fig. S1A in the ESI†).

A centimeter-sized thin film of mesoporous silica in MSTF⊥AAO can be routinely prepared (Fig. S1B in the ESI†). To confirm the macro-uniformity of the vertical mesopore channels over the entire MSTF membrane, we further examined the membrane by using grazing-incidence small-angle X-ray scattering (GISAXS). Three prominent spots on the left *x*-axis of the grazing-incidence X-ray beam can be seen in the 2D GISAXS pattern, and there is no structure along the *z*-direction (Fig. 1I). Fig. 1J shows the 1D GISAXS profile with the (100) (110) and (200) peaks, indicating that a highly ordered 2D hexagonal packing of vertical pores of the MSTF has been prepared. The 1D GISAXS profile gives a d-spacing of 6.5 nm, equivalent to a pore-to-pore centre distance of 7.5 nm, which is consistent with our SEM results (Fig. 1F) (average pore size of 5.4 ± 0.4 nm and pore wall sizes of 2.1 ± 0.2 nm). The highly ordered vertical nanochannels of the mesoporous thin film-MSTF can be therefore prepared over a large area. Meanwhile, the macroscopically continuous and non-breaking nature of materials has been confirmed.[11,12]

Given that the electrolyte wettability of a battery separator also correlates with the ion transport performance,[10] contact angle measurements are used to evaluate the wettability of electrolyte on the as-prepared membrane. The contact angle measurement of MSTF⊥AAO shows superior wettability with contact angle (CA) ≈ 0° in both 1 M LiTFSI DOL/DME electrolyte (Fig. 1K) and 1 M LiPF₆ EC-DEC electrolyte in the comparison of the Celgard 2325 and AAO membrane (Fig. S1C–H in the ESI†), indicating that the mesoporous MSTF membrane can achieve rapid absorption and diffusion of liquid electrolytes. Moreover, the excellent thermal stability of the MSTF⊥AAO membrane was examined by thermal gravimetric analysis (TGA) measurements under ambient air conditions (Fig. S1I in the ESI†). The vast thickness difference between AAO and the MSTF may result in an unnoticeable change in the TGA results. Thus, we performed TGA of pore-expanded mesoporous silica nanoparticles (ex-MSN) which is a concomitant product with the same silica mesostructure as the MSTF. The TGA results also suggest the good thermal stability of ex-MSN up to 600 °C (Fig. S1J in the ESI†). Zeta
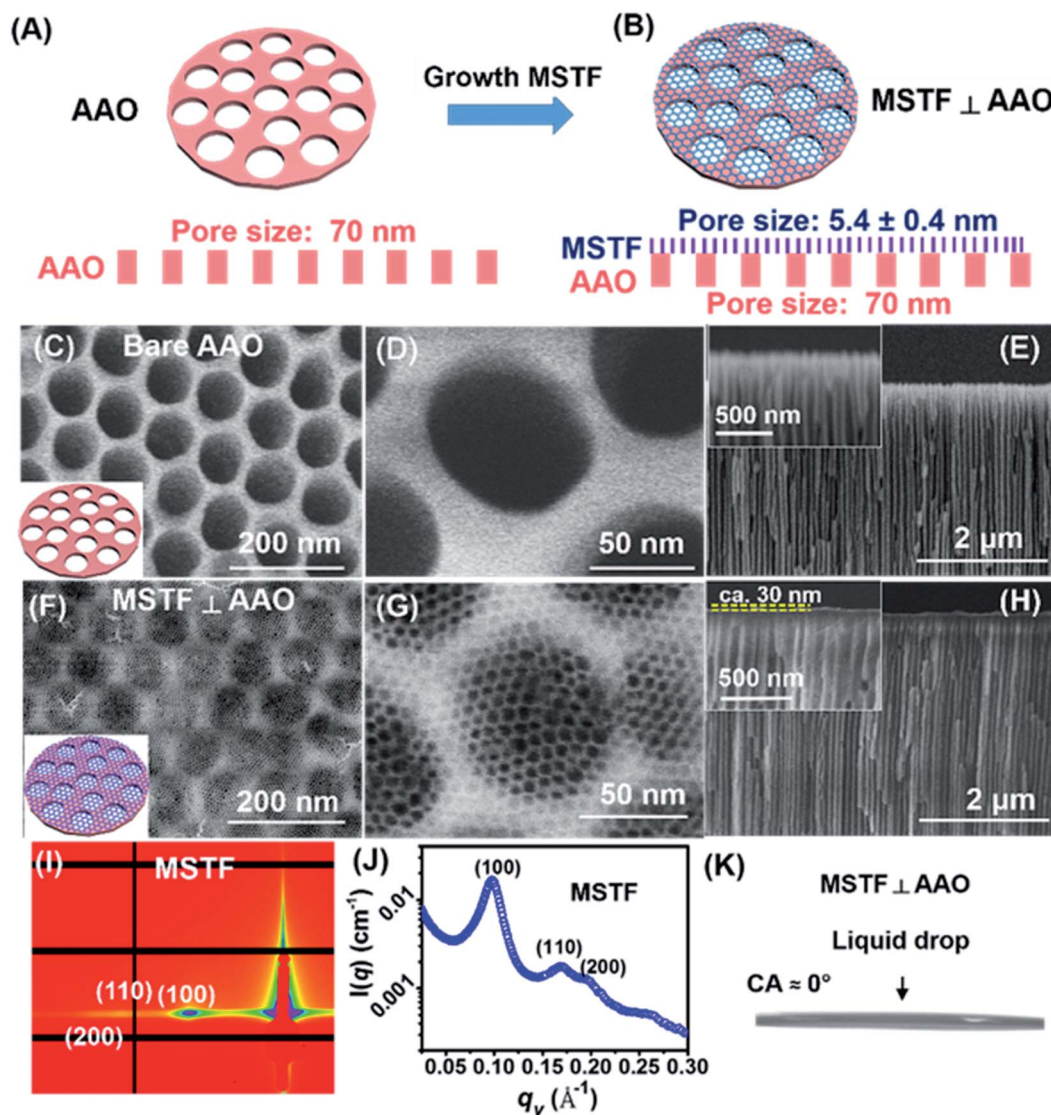
5096 | *J. Mater. Chem. A*, 2020, **8**, 5095–5104

This journal is © The Royal Society of Chemistry 2020

Fig. 1 Schematic diagram and morphology characterization of the AAO separator and MSTF⊥AAO separator. A schematic of the (A) AAO separator and (B) MSTF⊥AAO separator. SEM images of the surface and cross-section of (C–E) bare AAO film and (F–H) MSTF on the AAO film. (I) 2D GISAXS scattering profile and (J) 1D intensity profile plotted against q_y for the GISAXS pattern of the MSTF thin membrane. (K) Contact angle image of the MSTF⊥AAO film. The electrolyte is 1 M LiTFSI in 1 : 1 (v/v) solution of DOL/DME.

potential measurements show that the MSTF membrane is negatively charged which has been reported as an effective strategy to stabilize Li deposition.[13] (Fig. S1K in the ESI†) Thus, the MSTF⊥AAO membrane has several features such as uniform nanochannels (high porosity, tortuosity ≈ 1), great affinity with the electrolyte (CA ≈ 0°), high thermal stability, and a negatively charged surface which are the requirements of next-generation separators.

In order to examine the effect of the MSTF⊥AAO nanoporous separator on the Li deposition behavior, we investigated the behavior of Li electroplating and electrostripping with the nanoporous separator using galvanostatic cycling of Li–Li symmetric cells in the liquid electrolyte as shown in Fig. 2A. Fig. 2B shows the galvanostatic cycling performance of the Li–Li symmetric cell with Celgard 2325 (black), bare AAO (red) and

the MSTF⊥AAO separator (blue) cycled at a fixed current density of 2 mA cm^{-2} and capacity of 1 mA h cm^{-2}. The cell with the MSTF⊥AAO separator gives an excellent cycling stability with stable voltage polarization for over 2000 h of operation, suggesting that Li cycling is highly stable and reversible with the MSTF⊥AAO separator, and Li dendrite growth is dramatically suppressed. The overpotential of the Li plating/stripping process obtained with bare AAO and MSTF⊥AAO separators is high in the initial cycles (<20 h), suggesting that the electrochemical behavior of Li metal is unstable. After the initial cycles, the overpotential of the Li plating/stripping process becomes stable which could result from the formation of suitable SEI layers. Also, the formation of stable inorganic separator-Li metal interfaces should be taken into consideration.
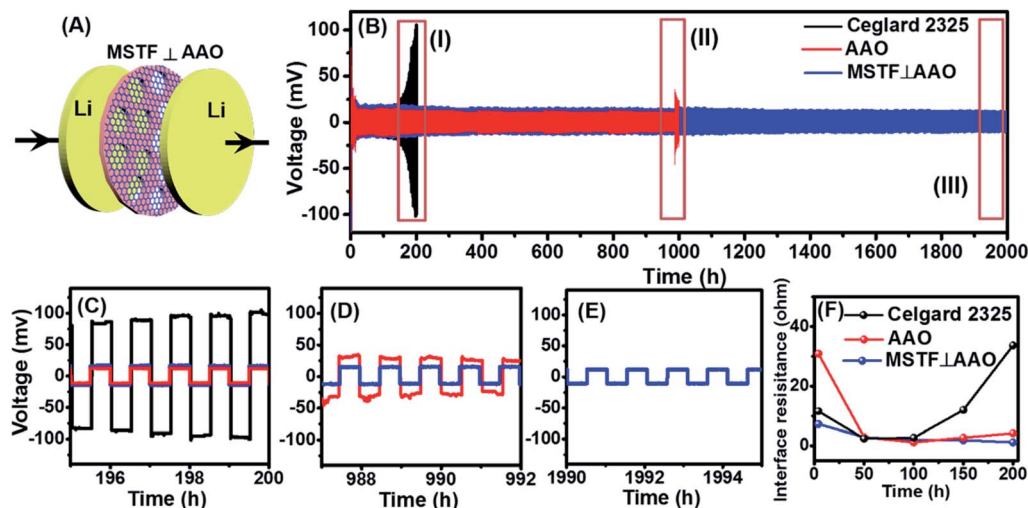
Fig. 2 Electrochemical tests with MSTF⊥AAO, bare AAO and the Celgard 2325 separator. (A) Schematic of the symmetric cell for the lithium plating/stripping experiment. (B) Galvanostatic cycling performance of the Li–Li symmetric cell with (blue) MSTF⊥AAO, (red) bare AAO and (black) Celgard 2325 separator cycled at a fixed current density of 2 mA cm^{-2} and capacity of 1 mA h cm^{-2}, (C–E) the galvanostatic cycling profile of cycling regions (I)–(III) shown in (B). (F) Interfacial resistance of Li metal in Li–Li symmetric cells calculated from impedance spectra after cycling. The electrolyte is 1 M LiTFSI in a 1 : 1 (v/v) solution of DOL/DME.

Fig. 2C–E show the galvanostatic cycling profiles of operation regions (I)–(III) shown in Fig. 2B. The overpotential of Li plating/stripping behavior obtained with the MSTF⊥AAO separator shows a low overpotential of ∼22 mV. In contrast, the voltage profiles obtained in the Li–Li symmetric cell with the Celgard 2325 separator exhibit a dramatic increase in the overpotential of Li plating/stripping in less than 200 h of operation which is attributed to the instability of Li/electrolyte interfaces (Fig. 2C). The cell with the bare AAO separator shows an overpotential of ∼20 mV and the voltage for the Li plating/stripping extremely increases in about 1000 h of operation (Fig. 2D), indicating that cell failure happened. The cycling performance of Li–Li symmetric cells with the Celgard 2325 and AAO separator is consistent with previous results.[14] The cycling performance of Li–Li symmetric cells with the MSTF⊥AAO separator exhibits a great improvement over the previous studies summarized in Table S1.†

The stability of the Li metal/electrolyte interface was evaluated using electrochemical impedance spectroscopy (EIS) to provide additional insight into the role of the nanoporous separator in Li metal batteries.[15] The EIS results show that the cells with AAO and MSTF⊥AAO separators exhibit less variation of interfacial impedance (R_{SEI}) than that of the Celgard 2325 separator, indicating that more stable SEI layers are formed with the AAO and MSTF⊥AAO separator after 50 cycles (Fig. 2F and S2†).

To further understand the effect of the MSTF⊥AAO separator on the suppression of Li dendrites during the Li plating/stripping process, the SEM observation of the morphologies of the Li metal surface after cycles was performed. The Li metal in the cells stopped at the end of the stripping process was used for the SEM measurements. SEM images of the Li metal surface cycled with Celgard 2325 after 200 cycles and AAO separators after 400 cycles show extensive appearance of micrometer-sized

and tree-like structures (Fig. 3A–D), suggesting the formation of Li dendritic structures after cycling.[16] In contrast, Li metal cycled with the MSTF⊥AAO separator shows a dendrite-free flat surface which is correlated to stable Li cycling performance obtained in the Li–Li symmetric cell (Fig. 3E, F). Fig. S3A, B† show SEM images of Li metal cycled with the MSTF side and AAO side of the MSTF⊥AAO separator at a fixed current density of 2 mA cm^{-2} and capacity of 1 mA h cm^{-2}. Uniform Li deposition can be achieved in the MSTF side of the MSTF⊥AAO separator. SEM images of the MSTF⊥AAO separator show that the MSTF remained on the AAO surface and has high electrochemical stability after cycling (Fig. S3C–G in the ESI†).

We next examine the penetration of lithium into the AAO channels after cycling with synchrotron transmission X-ray microscopy (TXM). Fig. 3G shows that the TXM image of AAO before cycling exhibits uniform and hollow channels (marked by red arrow). Fig. 3H–I show the TXM images of AAO and MSTF⊥AAO separators cycled at a fixed current density of 2 mA cm^{-2} and capacity of 1 mA h cm^{-2} after 400 repeated Li plating–stripping cycles, respectively. In Fig. 3H, bright channels with ∼400 nm width in the AAO separator pointed by white arrow suggest that residual Li metal is present in the channels of AAO after cycling which is associated with deep penetration of Li dendrites and eventual cell failure. Movie S1† shows the corresponding TXM movie of the AAO separator after cycling. In contrast, the MSTF⊥AAO separator as shown in the TXM image (Fig. 3I) shows no residual Li in MSTF⊥AAO separators after 400 cycles, which suggests that the MSTF⊥AAO separator is able to block the Li penetration.[17] Fig. S3H† shows the TXM image of MSTF⊥AAO separators before cycling.

To further evaluate the electrochemical compatibility of the MSTF⊥AAO membrane with the Li metal at high current densities, galvanostatic Li cycling experiments at higher current densities were performed in the ether-based electrolyte system
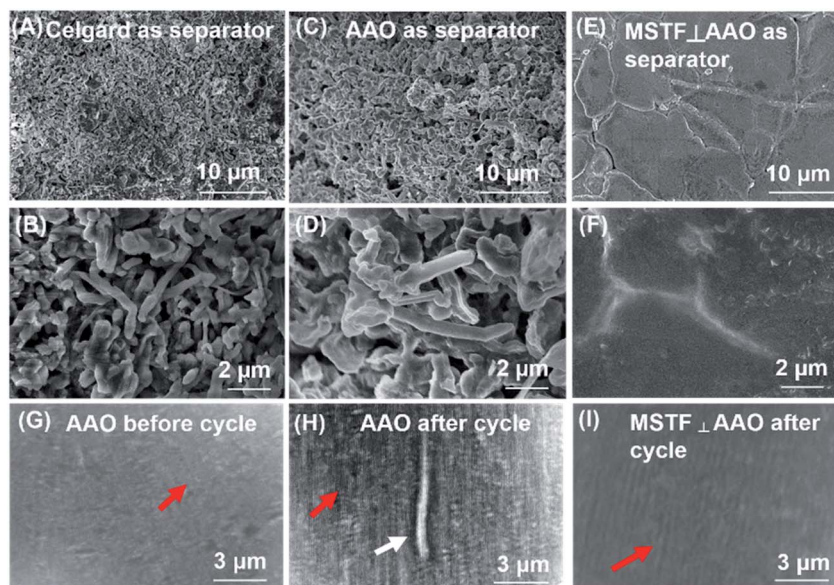
Fig. 3 Li morphologies of Li–Li symmetrical cells after Li plating–stripping cycles. The surface SEM image of Li metal cycled in a Li–Li symmetric cell with (A and B) Celgard 2325 at a fixed current density of 2 mA cm^{-2} and capacity of 1 mA h cm^{-2} after 200 repeated Li plating–stripping cycles and (C and D) bare AAO and (E and F) MSTF⊥AAO separator at a fixed current density of 2 mA cm^{-2} and capacity of 1 mA h cm^{-2} after 400 repeated Li plating–stripping cycles. The Li metal was stopped at the end of the stripping process. (G) TXM image of bare AAO. TXM images of (H) AAO and (I) MSTF⊥AAO separator cycled at a fixed current density of 2 mA cm^{-2} and capacity of 1 mA h cm^{-2} after 400 repeated Li plating–stripping cycles, respectively. The electrolyte is 1 M LiTFSI in a 1 : 1 (v/v) solution of DOL/DME.

(Fig. 4A–C). At a fixed current density of 3 mA cm^{-2} and capacity of 1.5 mA h cm^{-2}, the voltage profiles obtained with the MSTF⊥AAO separator maintain lower overpotential (15–25 mV) and have an ultra-long cycling life in comparison with the AAO separator (150–230 mV) for even more than 2000 h of operation (Fig. 4A). At a very high current density 10 mA cm^{-2} and capacity
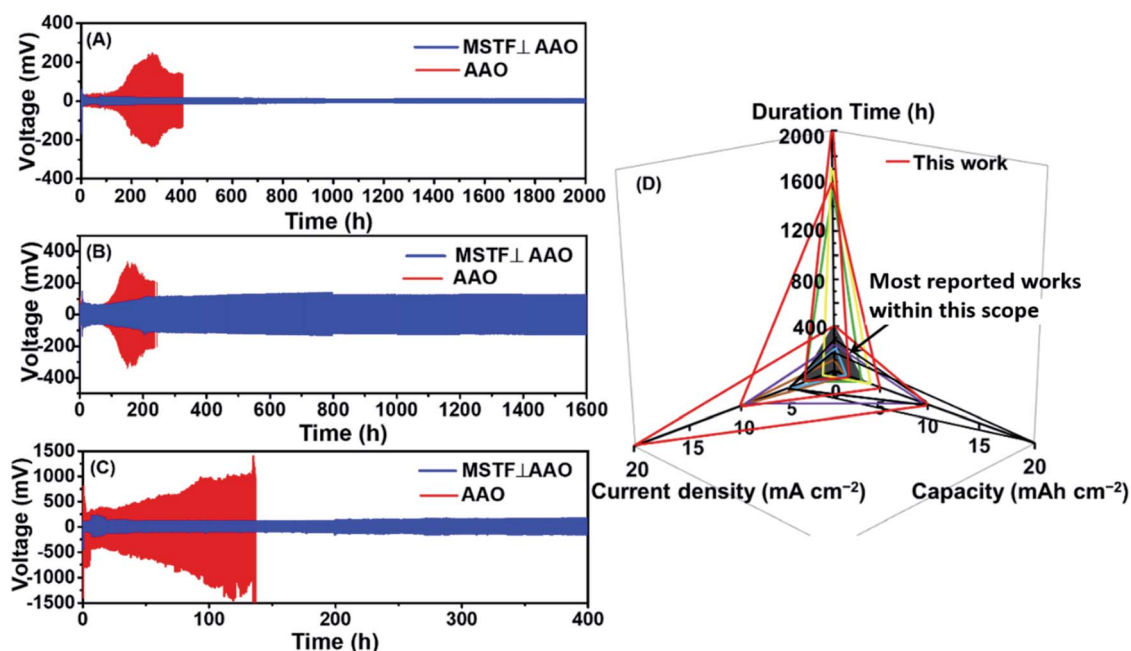

Fig. 4 Electrochemical properties with MSTF⊥AAO, bare AAO as the separator at high current densities and comparison of electrochemical performance indices. The galvanostatic cycling performance of Li–Li symmetric cells with bare AAO (red line) and MSTF⊥AAO (blue line) at fixed current densities of (A) 3 mA cm^{-2} and capacity of 1.5 mA h cm^{-2}, (B) 10 mA cm^{-2} and capacity of 5 mA h cm^{-2}, and (C) 20 mA cm^{-2} and capacity of 10 mA h cm^{-2}. The electrolyte is 1 M LiTFSI in a 1 : 1 (v/v) solution of DOL/DME. (D) Comparison of electrochemical performance indices (current density, capacity, and duration time), as measured in the Li–Li asymmetric cells with the MSTF⊥AAO (red) separator with those reported in the literature (a total of 9 entries as summarized in Table S1†).

Journal of Materials Chemistry A

Paper

of 5 mA h cm^{-2}, the MSTF⊥AAO separator could maintain stable cycles for more than 1600 h of operation without a short circuit (Fig. 4B), while overpotential obtained with the AAO separator suddenly drops after approximately 250 h of cycling which is attributed to short circuits. Significantly, for an extremely high current density of 20 mA cm^{-2} and capacity of 10 mA h cm^{-2}, stable Li cycling can even be achieved with the MSTF⊥AAO separator for over 400 h of operation with a low overpotential of 100–145 mV (Fig. 4C). However, the over-potential obtained with the corresponding bare AAO separator exhibits voltage fluctuations and shorts at ~135 h of cycling. Detailed voltage profiles are shown in Fig. S4 (ESI†). The pronounced enhancement of cycling performance with the MSTF⊥AAO separator can also be observed in the carbonate-based electrolyte system (Fig. S5A, B in the ESI†).

Moreover, Li metal cycled with the MSTF side and AAO side of the MSTF⊥AAO separator at higher current density was further examined using SEM (Fig. S5C, D in the ESI†). The SEM images show that the MSTF regulates the Li plating/stripping processes and suppresses the formation of Li dendrites. Fig. 4D and Table S1† show the performance of the MSTF⊥AAO separator in the Li–Li symmetric cells compared with other reported results.[18–26] Given that capacity, current density, and duration time are all the key parameters to evaluate the stability of the Li plating/stripping process, many studies reported good battery performance only with one or two indicators. Thus, the three dimensional coordinate diagram shown in Fig. 4D was applied to compare the performance of the MSTF⊥AAO separator (red line) with other reported studies in Li–Li cells, in which most reported studies are limited to the cycling conditions within the scope of current density under 2 mA cm^{-2}, capacity under 2 mA h cm^{-2} and duration time under 400 h (the black shaded area labeled in Fig. 4D). Although Li–Li symmetric cells cycled at a high current density of 5 mA cm^{-2} and high capacity of 20 mA h cm^{-2} have been previously demonstrated, the duration time only lasted for 180 h. Our MSTF⊥AAO separator shows such a long cycle life and high stability at high current densities and capacities, which are superior to those of previous reports (Fig. 4D and Table S1†).[18–26]

We next discuss possible reasons for the stable Li plating/stripping process with the MSTF⊥AAO separator. First, Li metal forms dendrites at the Sand's time when the current density reaches over-limiting current.[27,28] During the Li deposition process, the depleted Li ions near the electrode surface are unable to be replenished by the diffusion process. Thus, concentration gradients lead to the formation of space-charge region and Li dendrites. Previous studies show that the formation of Li dendrites can be suppressed under some conditions such as low current density and high Li$^+$ transference number (t_{Li+}).[2,13,27] Based on the Peers equation,[29] the limiting current-density in the electrode (J_{lim}) can be written (the detailed derivation of the Peers equation is listed in the ESI†):

$$J_{lim} = Z_c C_0 F \Phi (D_{solution}) (\tau)^{-1} (L)^{-1} (t_-)^{-1} \qquad (1)$$

where Z_c is the charge number of the lithium cation ($Z_c = 1$), C_0 is the bulk electrolyte concentration ($C_0 = 1$), F is the Faraday constant, Φ is the volume fraction of void, $D_{solution}$ is the diffusion coefficient of solution, τ is the tortuosity of the diffusion path, L is the thickness of the separator, and t_- is the transference number of anions. The detailed derivation of the Peers equation is provided in the ESI.† The tortuosity factor of Celgard 2325[30] is about 2.5 times higher than the tortuosity factor of the MSTF⊥AAO separator. (see the ESI†) According to eqn (1), the MSTF⊥AAO separator could tolerate ~2.5 times higher limiting current density than the Celgard 2325 separator with a similar thickness and volume fraction of void. Second, the use of an immobilized anion on the electrode surface has been shown to stabilize Li deposition.[31] As the MSTF materials being highly negatively charged and immobile, tuning pore size to meet the Debye length of the electrolyte can regulate the t_{Li+} to nearly unity. The proposed MSTF structure with both small pore and highly negatively charged channels can exclude the transport of anions and decrease the t_- value to nearly zero.[13,31,32] According to eqn (1), the MSTF⊥AAO separator with a very small t_- should give a much higher J_{lim}. In our previous work, both experimental results and theoretical calculation showed that the MSTF⊥AAO membrane with a uniform and periodic perpendicular pore structure can achieve ultra-high permeate flux in ultrafiltration.[12] The concept of permeability can also be applied to theoretically evaluate the Li$^+$-ion transport in the separator membrane.[10] Third, the MSTF with a small pore size (5.4 ± 0.4 nm) can easily block even the nanometer-sized Li dendrite structure. Fourth, Monroe et al. reported that a mechanically strong separator can be used to suppress the formation of Li dendrites.[33] An inorganic MSTF⊥AAO separator with a high shear modulus can effectively suppress Li dendrites. Lastly, the fine spacing of the pore opening of the MSTF leads to a very uniform distribution of Li flux (along the x,y plane) during the Li deposition.

The cycling performance of Li–Cu asymmetric cells with the MSTF⊥AAO separator was investigated to quantify the stability of Li plating/stripping behavior resulted from the electrolyte/separator assembly.[7] Fig. 5A, B show that the Li–Cu asymmetric cells cycled with the MSTF⊥AAO separator exhibit a high CE of >99.9% with stable plating/stripping voltage profiles for more than 250 cycles at a current density of 10 mA cm^{-2}. Each plating and stripping process is 30 min. Such a high CE suggests that the Li plating/stripping process is highly reversible with the MSTF⊥AAO separator. The stable Li plating/stripping process can also be achieved at lower current density (Fig. S6 in the ESI†). The lower CE obtained with the MSTF⊥AAO separator at initial cycles could result from the formation of stable SEI layers occurred in the first 5 cycles. The cells cycled with the AAO separator exhibit an obvious fluctuation of CE, suggesting that the Li plating/stripping process is unstable. We then compare the performance of the MSTF⊥AAO separator with those reported in the literature.[22,34–45] The MSTF⊥AAO separator shows the advance over the state-of-the-art separator (Fig. 5C and Table S2†). A CE of at least 99.8% required for the future application of anode-free batteries (e.g., >100 cycles) has been proposed to withstand extensive cycling.[46]
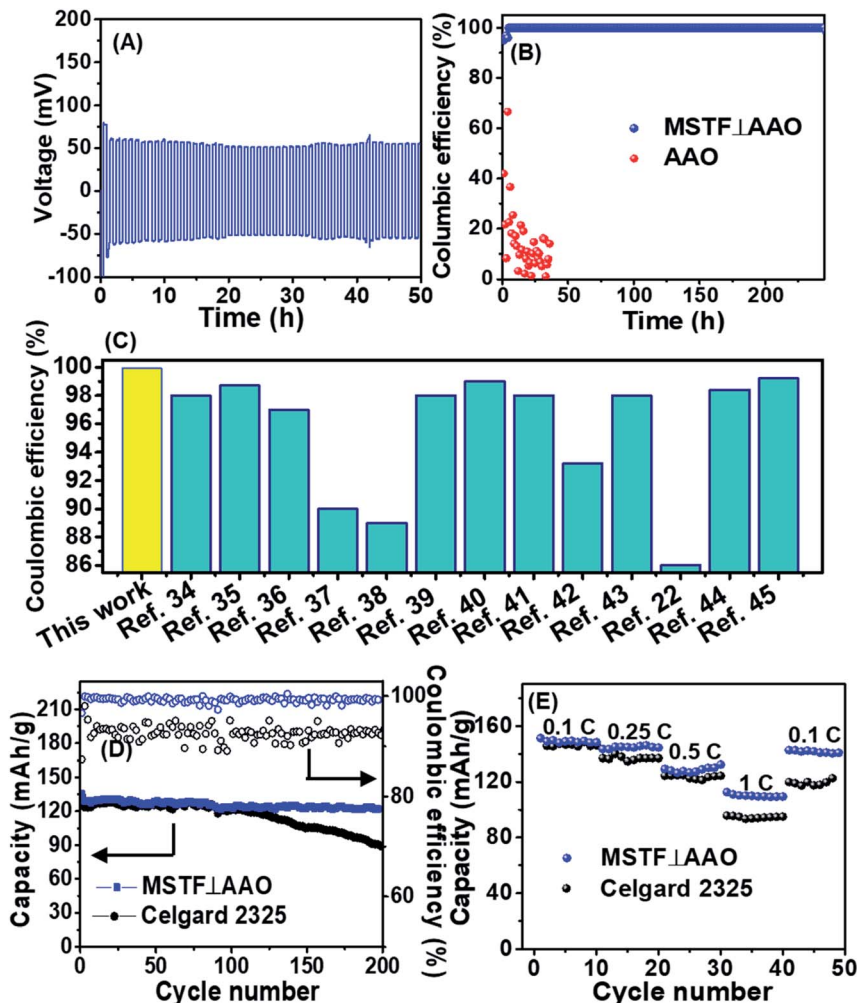
5100 | J. Mater. Chem. A, 2020, **8**, 5095–5104

This journal is © The Royal Society of Chemistry 2020

Fig. 5 (A) Galvanostatic cycling performance of the Li–Cu asymmetric cell with MSTF⊥AAO cycled at a fixed current density of 10 mA cm^{-2} and capacity of 5 mA h cm^{-2}. (B) Coulombic efficiency of the cell with bare AAO and MSTF⊥AAO cycled at a fixed current density of 10 mA cm^{-2} and capacity of 5 mA h cm^{-2}. Cu is against the MSTF side in cells with MSTF⊥AAO separators. The electrolyte is 1 M LiTFSI in a 1 : 1 (v/v) solution of DOL/DME. (C) Coulombic efficiency of a Li–Cu cell with the MSTF⊥AAO separator, compared with the coulombic efficiency of Li–Cu cells improved by various strategies (a total of 13 entries as summarized in Table S2†). (D) Cycling performance of Li/LiFePO$_4$ batteries with the Celgard 2325 and MSTF⊥AAO separator, respectively. The C rate is 0.5C. (E) Cycling performance of Li/LiFePO$_4$ batteries with the Celgard 2325 and MSTF⊥AAO separator cycled at various C-rates.

An increase in CE from ∼99.0% (previous studies) to >99.9% (this study) suggests that formation of dead Li decreases by more than 10-fold during cycling. A high CE (>99.9%) is required for the development of next-generation batteries. Fig. S7† shows the surface and cross sectional SEM images of the Cu electrode cycled in Li–Cu asymmetric cells with the AAO and MSTF⊥AAO separator after 50 cycles and 150 cycles at a current density of 2 mA cm^{-2} and a capacity of 1 mA h cm^{-2}, respectively. The Cu surface cycled with the MSTF⊥AAO separator shows a clean and smooth Cu surface which is consistent with the excellent CE of Li–Cu cells shown in Fig. 5A, B.

We next perform a battery test with the Li metal anode, LFP cathode and MSTF⊥AAO separator. Fig. 5D shows the cycling performance of Li-LFP batteries with the MSTF⊥AAO separator and Celgard 2325 separator cycled at a 0.5C rate. An initial specific capacity of ∼130 mA h g^{-1} was observed with the

MSTF⊥AAO separator and the battery performance still maintains after 200 cycles with a CE of ∼99.6%, demonstrating that Li-metal, MSTF⊥AAO, and liquid electrolytes are compatible. Meanwhile, the decrease in Li-LFP battery performance with the MSTF⊥AAO separator is slower than that with the Celgard 2325 separator. Furthermore, our separator exhibits stable battery performance at various C rates (Fig. 5E). The battery displays a capacity of ∼150 mA h g^{-1} at 0.1C and ∼110 mA h g^{-1} at 1C, whereas the capacities obtained from the cells with bare Celgard 2325 shows a significant decrease of the specific capacity of ∼145 mA h g^{-1} at 0.1C and ∼95 mA h g^{-1} at 1C. Notably, the batteries with the MSTF⊥AAO separator also show a capacity of ca. 100 mA h g^{-1} after 100 cycles and CE of ∼99.5% at a current density of 10C (Fig. S9 in the ESI†). Thus, the MSTF⊥AAO can significantly improve the charge–discharge rate performance of Li metal batteries.
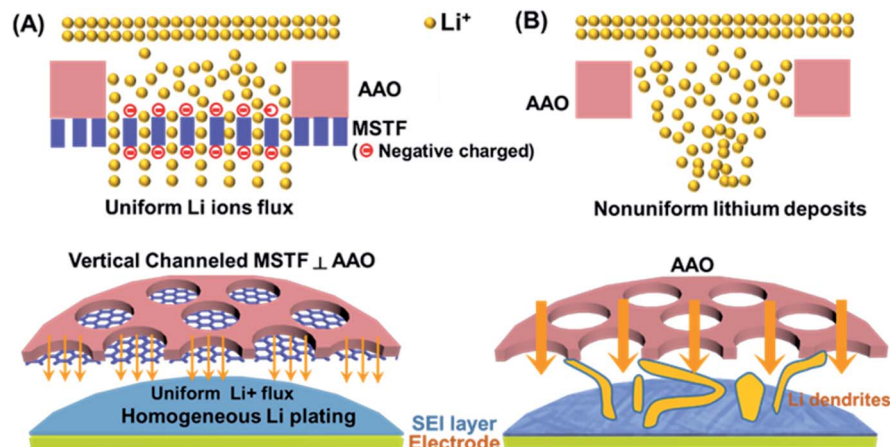
Fig. 6 Li deposition mechanism. A schematic figure of Li deposition on the electrode through (A) MSTF⊥AAO separator and (B) AAO separator.

According to the aforementioned results, the MSTF⊥AAO separator exhibits excellent cycling performance of Li–Li cells and Li–Cu cells and suppresses the formation of Li dendrites at ultra-high current densities. Correlating the experimental results with the properties of the MSTF⊥AAO separator, the proposed dendrite-resistant mechanism is shown schematically in Fig. 6. First, the fine spacing of the uniform mesopore (5.4 ± 0.4 nm) opening in the MSTF acts as a Li ion redistributor to regulate the Li^+ flux and leads to a very uniform Li^+ distribution (along the x,y, plane) and thus uniforms Li plating. Second, the MSTF⊥AAO membrane with negatively charged perpendicular nanochannels and low tortuosity ($\tau \approx 1$) can promote uniformity of ion distribution in the z-direction due to the high transference number of lithium ions moving in the nanochannels of the MSTF which prevent the formation of Li dendrites. Third, the strong mechanical properties of the MSTF⊥AAO separator block the Li whisker penetration or punching through the separator. Furthermore, the periodic-patterned MSTF could serve as a good model system to understand the electrochemical dynamics during cycling. However a disadvantage of AAO as the separator is its brittleness owing to the lack of active plastic deformation mechanisms. This problem may be dealt with in two directions. First, our newly developed transfer method for making MSTF⊥AAO, in contrast to the direct growth process in our previous work,[12] would allow us to transfer the MSTF to other porous polymer films to make a ductile MSTF/polymer, such as PVDF or PE, which is under investigation in our laboratory. Second, recent work has shown that a highly ductile dense amorphous aluminium oxide film at room temperature and a high strain rate can be obtained by a special fabrication process.[48] This gives hope for developing a ductile porous aluminium oxide film in the future.

Conclusions

In summary, we have developed a superior dendrite-resistant MSTF⊥AAO membrane with negatively charged uniform perpendicular nanochannels (5.4 ± 0.4 nm), good electrolyte wettability (CA ≈ 0°), high thermal stability and strong mechanical properties as an effective dendrite-free separator for stable Li plating–stripping processes. The effect of the MSTF⊥AAO membrane on the Li plating–stripping process has been systematically investigated. Excellent cycling performance can be achieved in Li–Li cells with the MSTF⊥AAO separator cycled at ultrahigh current densities such as 10 mA cm^{-2} for more than 1600 h of operation. Also, the MSTF⊥AAO separator results in the extremely high CE of >99.9% in Li–Cu cells cycled at a high current density of 10 mA cm^{-2} and capacity of 5 mA h cm^{-2} for more than 250 h of cycling. Full-cell Li metal battery tests suggest that the MSTF⊥AAO membrane can be used to achieve safe Li metal batteries. The rational design of the nanoporous solid membrane demonstrates homogeneous Li deposition and long lifetime performance for Li metal batteries.

Experimental section

Synthesis of the MSTF⊥AAO membrane

First, a thin polyvinylidene fluoride (PVDF) film was formed by spinning coating PVDF solution on a glass sheet (2 × 4 cm^2), and the PVDF film was used as a transfer layer to transfer the MSTF onto the porous anodic aluminium oxide membrane (AAO). Subsequently, the MSTF was grown on the PVDF film by the growth procedure of MSTFs reported previously.[11] Finally, the MSTF/PVDF layer was transferred on the AAO (pore size of 70 nm, thickness of 56 μm, Shengzheng Topmembrane Co. LTD., China) substrate and calcined in an air atmosphere at 500 °C to remove the PVDF interlayer. The MSTF⊥AAO synthesis method used in the present study has been significantly improved in the comparison of the synthesis method in our previous nanofiltration study.[12] Detailed information is in the ESI.†

Materials characterization and electrochemical measurements

Top-view and edge-view micrographs were recorded using a field emission SEM (Hitachi S-4800) which operated at

5102 | *J. Mater. Chem. A*, 2020, **8**, 5095–5104

This journal is © The Royal Society of Chemistry 2020

accelerating voltages of 5 kV. Grazing-incidence small-angle X-ray scattering (GISAXS) was conducted at the BL23A station in Taiwan Light Source (TLS), National Synchrotron Radiation Research Center (NSRRC), Taiwan. The transmission X-ray microscopy (TXM) results were obtained at the BL01B1 beamline of TLS (NSRRC, Taiwan).[47] Contact angle measurements were performed with a contact angle goniometer (FTA125). Cycling processes were carried out by using an Arbin battery tester (Model BT 2043, Arbin Instruments Corp., USA) and electrochemical impedance spectroscopy (EIS) measurements were conducted using a frequency analyzer (Solartron 1255, AMETEK) in a frequency range from 0.01 Hz to 1 MHz with an amplitude of 10 mV and a potentiostat (Solartron 1287, AMETEK). Detailed information of electrochemical measurements is in the ESI.†

Electrolyte and cell preparation

The electrolytes were 1 M lithium bis(trifluoromethane sulfonyl)imide (LiTFSI) in a 1 : 1 (v/v) solution of 1,2-dimethoxyethane (DME)/1,3-dioxolane (DOL, anhydrous, Sigma-Aldrich) and 1 M lithium hexafluorophosphate in a 1 : 1 (v/v) solution of ethylene carbonate (EC) and diethyl carbonate (DEC). All the cells were assembled in an Ar-filled glove box with moisture and oxygen levels below 1 ppm. Detailed information is in the ESI.†

Conflicts of interest

There are no conflicts to declare.

Acknowledgements

References

1 X.-B. Cheng, R. Zhang, C.-Z. Zhao and Q. Zhang, *Chem. Rev.*, 2017, **117**, 10403–10473.

2 M. D. Tikekar, S. Choudhury, Z. Tu and L. A. Archer, *Nat. Energy*, 2016, **1**, 16114.

3 Y. Zhang, Z. Mu, J. Lai, Y. Chao, Y. Yang, P. Zhou, Y. Li, W. Yang, Z. Xia and S. Guo, *ACS Nano*, 2019, **13**, 2167–2175.

4 D. Lin, Y. Liu and Y. Cui, *Nat. Nanotechnol.*, 2017, **12**, 194.

5 Y. Xiang, J. Li, J. Lei, D. Liu, Z. Xie, D. Qu, K. Li, T. Deng and H. Tang, *ChemSusChem*, 2016, **9**, 3023–3039.

6 H.-L. Wu, L. A. Huff and A. A. Gewirth, *ACS Appl. Mater. Interfaces*, 2015, **7**, 1709–1719.

7 S. Chen, J. Zheng, D. Mei, K. S. Han, M. H. Engelhard, W. Zhao, W. Xu, J. Liu and J.-G. Zhang, *Adv. Mater.*, 2018, **30**, 1706102.

8 H.-L. Wu, M. Shin, Y.-M. Liu, K. A. See and A. A. Gewirth, *Nano Energy*, 2017, **32**, 50–58.

9 Y. Lu, Z. Tu and L. A. Archer, *Nat. Mater.*, 2014, **13**, 961.

10 M. F. Lagadec, R. Zahn and V. Wood, *Nat. Energy*, 2019, **4**, 16–25.

11 K.-C. Kao, C.-H. Lin, T.-Y. Chen, Y.-H. Liu and C.-Y. Mou, *J. Am. Chem. Soc.*, 2015, **137**, 3779–3782.

12 J. Yang, G.-S. Lin, C.-Y. Mou and K.-L. Tung, *Chem. Mater.*, 2019, **31**, 1745–1751.

13 J. L. Schaefer, D. A. Yanga and L. A. Archer, *Chem. Mater.*, 2013, **25**, 834–839.

14 Q. Lu, Y.-B. He, Q. Yu, B. Li, Y. V. Kaneti, Y. Yao, F. Kang and Q.-H. Yang, *Adv. Mater.*, 2017, **29**, 1604460.

15 R. Bouchet, S. Lascaud and M. Rosso, *J. Electrochem. Soc.*, 2003, **150**, A1385–A1389.

16 F. Ding, W. Xu, G. L. Graff, J. Zhang, M. L. Sushko, X. Chen, Y. Shao, M. H. Engelhard, Z. Nie, J. Xiao, X. Liu, P. V. Sushko, J. Liu and J.-G. Zhang, *J. Am. Chem. Soc.*, 2013, **135**, 4450–4456.

17 J.-H. Cheng, A. A. Assegie, C.-J. Huang, M.-H. Lin, A. M. Tripathi, C.-C. Wang, M.-T. Tang, Y.-F. Song, W.-N. Su and B. J. Hwang, *J. Phys. Chem. C*, 2017, **121**, 7761–7766.

18 Z. Tu, M. J. Zachman, S. Choudhury, S. Wei, L. Ma, Y. Yang, L. F. Kourkoutis and L. A. Archer, *Adv. Energy Mater.*, 2017, **7**, 1602367.

19 T. Dong, J. Zhang, G. Xu, J. Chai, H. Du, L. Wang, H. Wen, X. Zang, A. Du and Q. Jia, *Energy Environ. Sci.*, 2018, **11**, 1197–1203.

20 Q. Shi, Y. Zhong, M. Wu, H. Wang and H. Wang, *Proc. Natl. Acad. Sci. U. S. A.*, 2018, **115**, 5676–5680.

21 S. Choudhury and L. A. Archer, *Adv. Electron. Mater.*, 2016, **2**, 1500246.

22 S. S. Chi, Y. Liu, W. L. Song, L. Z. Fan and Q. Zhang, *Adv. Funct. Mater.*, 2017, **27**, 1700348.

23 C.-Z. Zhao, P.-Y. Chen, R. Zhang, X. Chen, B.-Q. Li, X.-Q. Zhang, X.-B. Cheng and Q. Zhang, *Sci. Adv.*, 2018, **4**, eaat3446.

24 H. Zhang, X. Liao, Y. Guan, Y. Xiang, M. Li, W. Zhang, X. Zhu, H. Ming, L. Lu and J. Qiu, *Nat. Commun.*, 2018, **9**, 3729.

25 Y. Li, Y. Li, Y. Sun, B. Butz, K. Yan, A. L. Koh, J. Zhao, A. Pei and Y. Cui, *Nano Lett.*, 2017, **17**, 5171–5178.

26 Z. Hu, S. Zhang, S. Dong, W. Li, H. Li, G. Cui and L. Chen, *Chem. Mater.*, 2017, **29**, 4682–4689.

27 P. Bai, J. Li, F. R. Brushett and M. Z. Bazant, *Energy Environ. Sci.*, 2016, **9**, 3221–3229.

28 P. Bai, J. Guo, M. Wang, A. Kushima, L. Su, J. Li, F. R. Brushett and M. Z. Bazant, *Joule*, 2018, **2**, 2434–2449.

This journal is © The Royal Society of Chemistry 2020

J. Mater. Chem. A, 2020, **8**, 5095–5104 | **5103**

29 T. HILL, *Membrane Phenomena-General Discussion*. Discussion of the faraday society. 1956, pp. 117–140.

30 D. P. Finegan, S. J. Cooper, B. Tjaden, O. O. Taiwo, J. Gelb, G. Hinds, D. J. L. Brett and P. R. Shearing, *J. Power Sources*, 2016, **333**, 184–192.

31 M. D. Tikekar, L. A. Archer and D. L. Koch, *J. Electrochem. Soc.*, 2014, **161**, A847–A855.

32 C. Yan, C. Lv, Y. Zhu, G. Chen, J. Sun and G. Yu, *Adv. Mater.*, 2017, **29**, 1703909.

33 C. Monroe and J. Newman, *J. Electrochem. Soc.*, 2005, **152**, A396–A404.

34 C. Li, S. Liu, C. Shi, G. Liang, Z. Lu, R. Fu and D. Wu, *Nat. Commun.*, 2019, **10**, 1363.

35 J. Luo, C. C. Fang and N. L. Wu, *Adv. Energy Mater.*, 2018, **8**, 1701482.

36 K. Liu, A. Pei, H. R. Lee, B. Kong, N. Liu, D. Lin, Y. Liu, C. Liu, P.-c. Hsu and Z. Bao, *J. Am. Chem. Soc.*, 2017, **139**, 4815–4820.

37 W. Liu, W. Li, D. Zhuo, G. Zheng, Z. Lu, K. Liu and Y. Cui, *ACS Cent. Sci.*, 2017, **3**, 135.

38 W. Liu, D. Lin, A. Pei and Y. Cui, *J. Am. Chem. Soc.*, 2016, **138**, 15443–15450.

39 Y. Liu, D. Lin, P. Y. Yuen, K. Liu, J. Xie, R. H. Dauskardt and Y. Cui, *Adv. Mater.*, 2017, **29**, 1605531.

40 T.-T. Zuo, Y.-X. Yin, S.-H. Wang, P.-F. Wang, X. Yang, J. Liu, C.-P. Yang and Y.-G. Guo, *Nano Lett.*, 2017, **18**, 297–301.

41 Y. Gao, Y. Zhao, Y. C. Li, Q. Huang, T. E. Mallouk and D. Wang, *J. Am. Chem. Soc.*, 2017, **139**, 15288–15291.

42 B. Zhu, Y. Jin, X. Hu, Q. Zheng, S. Zhang, Q. Wang and J. Zhu, *Adv. Mater.*, 2017, **29**, 1603755.

43 W. Zhang, H. L. Zhuang, L. Fan, L. Gao and Y. Lu, *Sci. Adv.*, 2018, **4**, eaar4410.

44 L. Fan, H. L. Zhuang, W. Zhang, Y. Fu, Z. Liao and Y. Lu, *Adv. Energy Mater.*, 2018, **8**, 1703360.

45 J. Xiang, L. Yuan, Y. Shen, Z. Cheng, K. Yuan, Z. Guo, Y. Zhang, X. Chen and Y. Huang, *Adv. Energy Mater.*, 2018, **8**, 1802352.

46 J. Qian, B. D. Adams, J. Zheng, W. Xu, W. A. Henderson, J. Wang, M. E. Bowden, S. Xu, J. Hu and J. G. Zhang, *Adv. Funct. Mater.*, 2016, **26**, 7094–7102.

47 C.-C. Wang, C.-C. Chiang, B. Liang, G.-C. Yin, Y.-T. Weng and L.-C. Wang, *Sci. Rep.*, 2017, **7**, 3691.

48 E. J. Frankberg, J. Kalikka, F. García Ferré, L. Joly-Pottuz, T. Salminen, J. Hintikka, M. Hokka, S. Koneti, T. Douillard, B. Le Saint, P. Kreiml, M. J. Cordill, T. Epicier, D. Stauffer, M. Vanazzi, L. Roiban, J. Akola, F. Di Fonzo, E. Levänen and K. Masenelli-Varlot, *Science*, 2019, **366**, 864–869.

5104 | *J. Mater. Chem. A*, 2020, **8**, 5095–5104

This journal is © The Royal Society of Chemistry 2020